Laboratoire de Physique Nucléaire et de Hautes Énergies
CNRS - IN2P3 - Universités Paris VI et VII

Optoelectronic tests for SNDICE

E. Barrelet

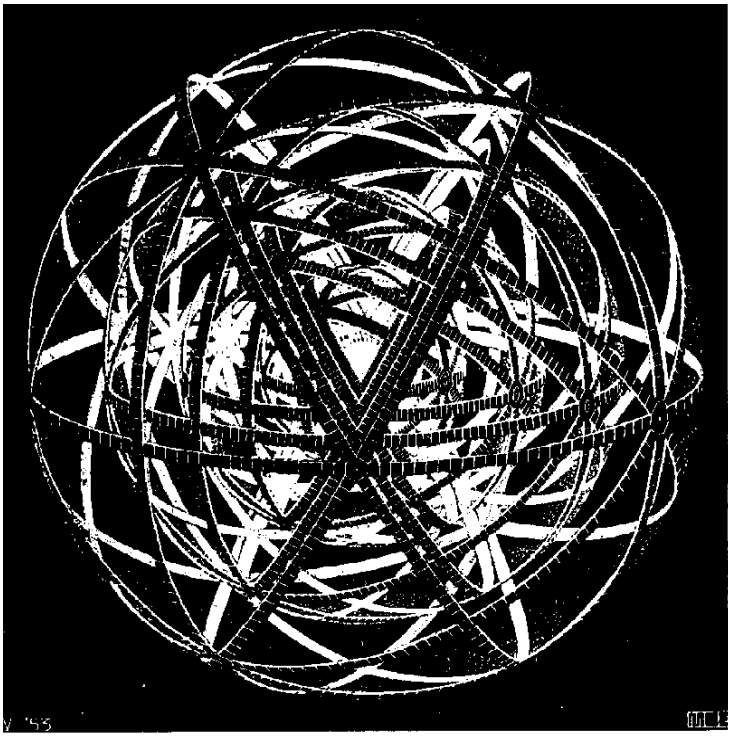

4, Place Jussieu - Tour 33 - Rez-de-Chaussée
75252 Paris Cedex 05
Tél.: 33(1) 44 27 63 13 - FAX: 33(1) 44 27 46 38

1 Introduction

We have gathered in this report the results of the tests involving only the SNDICE light source and one of the detectors used in SNDICE benches in a fixed position. In short in these tests one varies the led and the photodiode parameters (current, voltage and temperature). The underlying subject is the overall emission model of LEDs and the optimisation of their electronic control (the spectral distribution model was detailed in LPNHE 2009-01).
The test of the CLAP and its asic electronics belongs to this 'optoelectronic' type but it has been already the subject of a particular report (LPNHE 2007-04). These tests involving only the electronics -mainly noise measurements-, including dark currents, can be done in the electronic lab where electromagnetic interferences can be controled, but when they involve light propagation they are better done on the optical benches where respective positions and vibrations are better controled.

2 Methods used for the SNDICE optoelectronic tests

The mechanical setup of the test bench shown in Figure 1, is mainly our photometric test

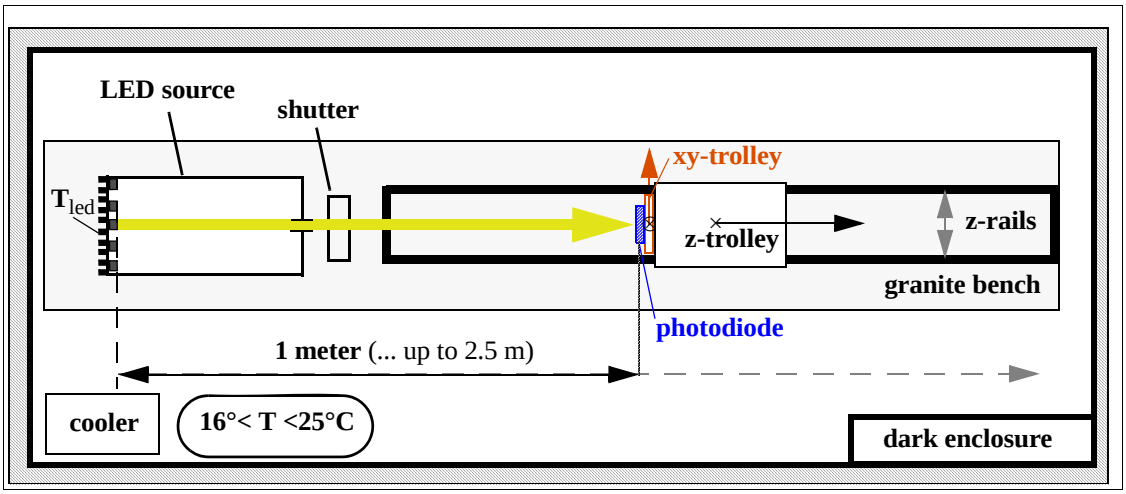

Figure 1: Top view of the calibration bench photometric setup used for optoelectronic tests. The position of the LED source and its light beam is figured by a thick yellow arrow.

bench setup. The light beam is defined by the LED dice and the exit circular hole of the led source. The detector x-y motion is used to center the detector on the beam of a given led and the z motion to vary the photon flux without changing the led or the photodiode status. An air cooler inside the dark enclosure can bring the inner bench temperature down to 16°C. The LEDs are passively cooled by a radiator connected to a temperature probe (monitored by the led backend electronic module). The calibrated photodiodes, at air temperature, are read by a feedback picoammeter (Keithley 6514) inside the dark enclosure. The CLAP photodiode, which is integrated in a frontend electronics box, is cooled by a Peltier module. Its temperature is independently monitored. The two «backend» electronics modules for leds and CLAPs stay outside the dark enclosure near the data acquisition PC.
The basic data collection runs consists of a periodic sampling of Led source signal,

photodiode signals and monitoring probes signals at different rates. The main modes are usually labeled «pedestal runs», «constant level runs» and «intensity ramps» and they can be declined as «constant temperature» or «variable temperature» runs.
The primary sampling period, from a fraction of second to a few seconds, is related to the sampling of the photodiode optical signal by a commercial picoammeter and the acquisition of an image by a CCD camera. A much faster period, a few microseconds for digitizing signals with a 16 bits precision, allows a characterization of noise sources, of the rise and fall time of optical signals and a use of averaging methods to increase precision. Much longer periods obtained by extending run duration to hours, days or weeks show the effects of temperature or other baseline drifts and environmental events or the lack of reliability of a subsystem. In short the «ramping» run modes focus on the dependance on a given variable while minimizing the effects of the multiplicity of small long term effects while «pedestal» and «level» runs tend to study these long term effects.

3 Testing the LED current generator

3.1 Overview of the LED electronics

Our LED control electronics is driven by a digital bus connected to a PC through a Digital Input-Out (DIO) interface card from National Instruments, which is programmed using LabView software. As shown in Figure 2, the digital part of the card is clocked by

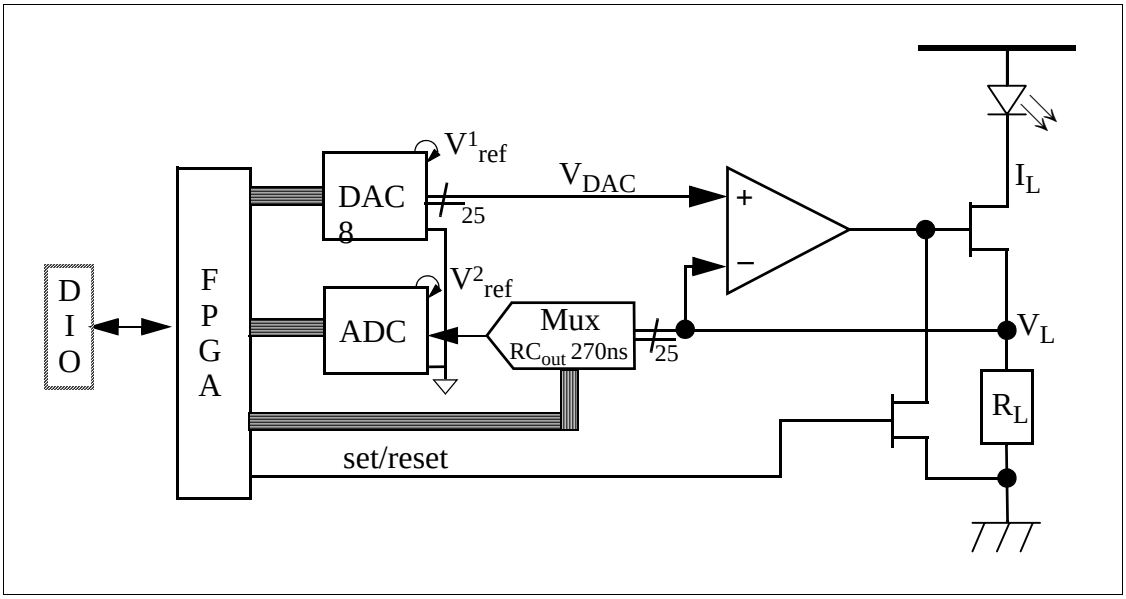

Figure 2: Schematic design of the “LED backend card”, showing the principle of the LED current control: the op-amp compares V_L with V_{DAC} and the transistor matches the current sense voltage V_L with V_{DAC}. The ADC samples V_L at a maximum rate of 500 khz and analyses precisely I_L.

a FPGA which loads two DAC circuits[1], one voltage channel for each LED controlled

[1] 2 AD5390: 16-channels, 14-bit voltage output

by a set/reset switch which yields light pulses with sharp rise and fall edges and suppresses residual light emission outside pulses. An ADC circuit[2] monitors the LED current wavefront in real time with a high precision. It is a key element of the quality analysis shown in next paragraph which demonstrate a potential for a $\leq 10^{-4}$ accuracy of our LED source. However the basic performances of our current sources rely on the quality of the COTS[3] components used in this card, namely: the voltage references of the ADC and DAC, the LED serial resistors R_L and the voltage division chains of ADC and DACs. An important detail is the choice of R_L values adapted to each LED, sorted in five categories according to the maximum current admitted from 20 mA to 0.5 A (cf. Table 1)

Name	<λ> (nm)	I_{max} (mA)	R_L (Ω) ($V_L \leq 1.25V$)[a]	Φ_{mid}/Φ_{std} (for megacam flat field)	LED category
GD2	480	500	2.5	26.34	overluminous
GD9	635	500	2.5	18.65	″
GD8	635	500	2.5	18.29	″
GD7	625	500	2.5	17.56	″
GD3	530	500	2.5	14.63	″
L400	405	350	3	14.63	″
GD6	470	500	2.5	13.17	″
GDIR	850	500	2.5	13.02	″
GD1	470	500	2.5	8.78	″
GD4	550	500	2.5	6.00	″
L420	425	350	3	5.85	″
GD5	590	500	2.5	2.93	″
L704	810	50	25	1.025	normal
L705	810	50	25	1.025	″
L701	735	50	25	0.977	″
L703	750	50	25	0.946	″
L950	950	100	12.5	0.732	″
L702	750	50	25	0.427	″
UV1	340	20	62	0.011	faint
UV3	340	20	62	0.009	″
UV0	310	20	62	0.005	″
UV2	310	20	62	0.004	″

Table 1: LED specific parameters : The standard flux Φ_{std} for a megacam flat field illumination is set at a photoelectron yield of 2.10^4 e^-/pix for a 10 s exposure. Φ_{mid} is the flux at mid I_{led} range.

a. for better precision DAC reference voltage V^{DAC}_{ref} will be fixed to 2.5 V and R_L will be doubled

The DAC reference voltage (V^{DAC}_{ref} in Figure 2) is either 1.25 or 2.5 volt (but the resistors R_L are matched to 1.25 volt). Each DAC output is $V_{out}^{i} = 1.25(2.5)*N^i/2^{14}$ (Volt) for a digital input N^i ($0 \leq N \leq 16383$). The DAC level step is 76.3(152.6) μV. The ADC is

[2] LTC1608: 16-bit, 500 ksample/s

[3] usual acronym for Commercial On The Shelf

differential. The negative analog input (A_{in}^-) and the DAC zero are grounded. The ADC reference voltage (V^2_{ref} in Figure 2) is 2.5 Volt. Consequently the DAC output range is mapped exactly on the half (or the whole) positive ADC range, i.e. on the codes 0 to 16383 (32767). In summary 1 DAC unit (1 dau) equals one (or two) ADC unit (1 adu=76.3 μV). Actually we had a third solution used during our first runs: a coefficient 1/2 on the DAC input and a 2.5 volt reference. The output is confined to a 1.25 range, therefore it is compatible with the 1.25 V resistor values, but it looses even codes and the apparent DAC unit equals 2 adu.

The noise associated with a successive approximation ADC (transition noise) is characterized by the "time domain histogram" obtained by digitizing a low noise DC level[4]. We shall see that our ADC monitoring noise is compatible with a gaussian white noise of width 0.8 adu (RMS). This is barely sufficient to extend our voltage monitoring range by averaging ADC samples. However this works : we shall be able by averaging to follow the LED current signal at a 0.05 adu level in the kiloherz frequency range and to study long term drift effects at a very low scale ($<0.3*10^{-6}$ part of maximum LED current).

3.1.1 Classification of LEDs according to Megacam response

The system described before allows to use the maximum LED intensity. For the more powerful LEDs with a 500 mA current and a 5% efficiency, this flux is excessive because it saturates an astronomic camera in a fraction of a second (LED labelled as overluminous in Table 1). This would not prevent us to specify a 10^{-4} precision for the system because the relevant LED illumination levels (~1000 adu) are very stable and are monitored within 0.1 adu. However it is reasonable to set a common reference calibration illumination level using practical considerations. Let us choose a reference flux yielding 10^3-10^4 e^-/pixel/s in a CCD which pixels cover (1 μrad)^2. Table 1 shows the actual fluxes for each LED in Megacam camera, relative to $\Phi_{std}= 2.10^3$ e^-/pixel/second, to be compared with the flux Φ_{mid} obtained at mid I_{LED} range. At a 1 m distance, a 1 cm^2 photodiode will yield a 10^8 times higher photocurrent, i.e. 16-160 nA (supposing that the CCD and the photodiode have the same quantum efficiency). At the other extremity of the calibration bench (2.5 m) the same LED intensity will yield a 3-30 nA and at the focal length distance (15 m) a 70-700 pA photocurrent.

In summary 200 nA is the typical photocurrent range for the calibration of the LED source (as a telescope direct illuminator) and 500 pA for the calibration a CCD camera (as a telescope focal plane). To understand the distinction between both calibration ranges, one has to remember that light intensity varies with the inverse square of the distance between the detector and the source, from the test bench to the telescope dimensions. It is shown in another report how the extension of our test bench to 15 meters validates this assumption -or more practically how it can extrapolate a photometric measurement at a 10^{-4} precision from the nanoampere range to the picoampere range.

---

[4] Its origin in LTC1608 is the gaussian noise of the input comparator working at 16 Mhz. It covers 3 successive adc codes (yielding a RMS ≈0.7 ADC unit).

3.2 Test of the LED electronics

3.2.1 LED current generator characteristic

The characteristic of the electronic circuit in Figure 2 (shown in Figure 3) is obtained

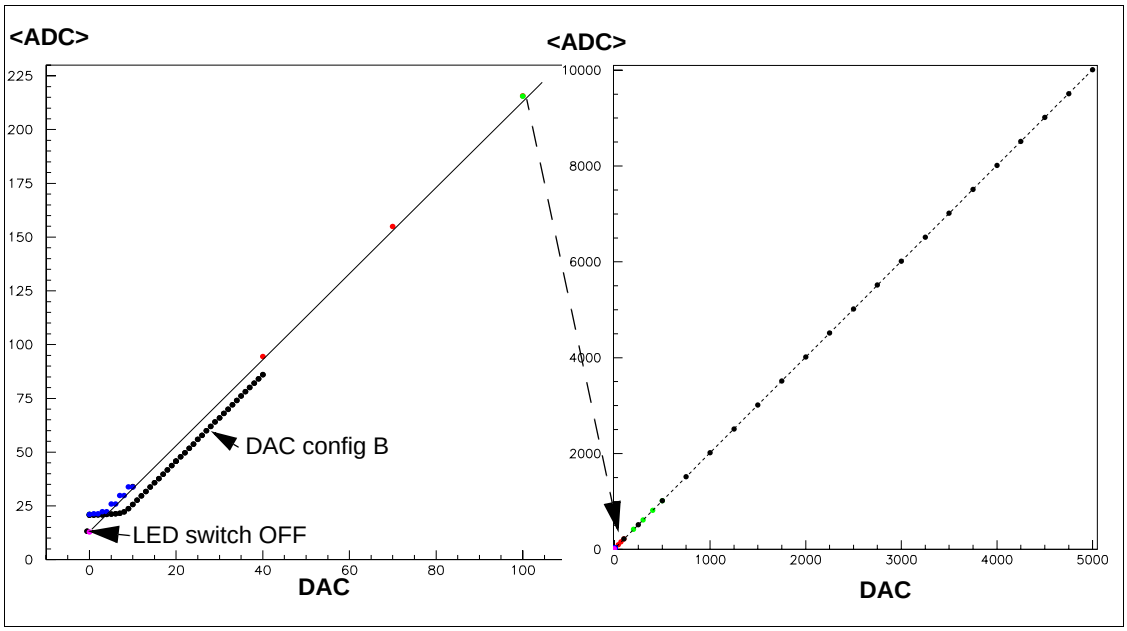

Figure 3: The mean value of 256 consecutive ADC samplings of V_L for a constant DAC count is itself averaged over a long period (around 40 minutes). The DAC count is ramped (left 0-10 blue and 10-100 red ramps; right same plus 0-500 green and 0-5000 black ramps). A linear fit accomodate data from DAC=10 to 5000 with residuals <±1 DAC unit and pass through the real zero current point obtained with LED-switch off. (DAC configurations : -A-(default) V^{DAC}_{ref} =2.5V and m=1/2; -B- V^{DAC}_{ref} =1.25V and m=1; -C- V^{DAC}_{ref} =2.5V and m=1. Dac digital input is first multiplied by m)

digitally by loading integer numbers in DAC first, then by reading a number N of ADC values (usually N=256) by computing their mean value and root mean square estimators and by repeating this operation. We are aware that highly leveraged signal averaging is potentially dangerous and must be controlled. We have reproduced in Appendix A an old report done for H1 experiment explaining how and why. Practically we have evaluated our electronic circuit by juxtaposing several ramps (DAC values 0-10, 10-100, 100-1000, 0-5000). Each step consists of a few hundred measurements of dark current level (led switch off) followed with a few thousand constant level measurements. The accuracy of our current scale is defined by the ADC reference voltage V^{ADC}_{ref} and the resistance R_F. and the quality of the level gradation from the DAC (but controlled by the ADC). According to the book, the electrical specifications of these components exceeds largely what is needed to assure the 10^{-4} stability and reproducibility of our light source at mid scale, if we assume a fixed relation between the electric led current and the emitted flux (what remains to be proven of course). The main result is that if we fit a straight line on that characteristic from DAC=10 to 5000, residuals are inferior to one DAC unit. That is even better than the specifications. The non-linearity near DAC=0 is due to the small analog offset of the dac output. Our plan is to slightly bias this output to

suppress this non linearity and to recover the missing levels corresponding virtually to 4 DAC codes. The ramp will then reach the led switch OFF point, which is on the straight line.

3.2.2 LED current generator fluctuations

We represent the fluctuation of the measured LED current with a three component noise model described in Figure 4. It is due more to the measurement apparatus than to the

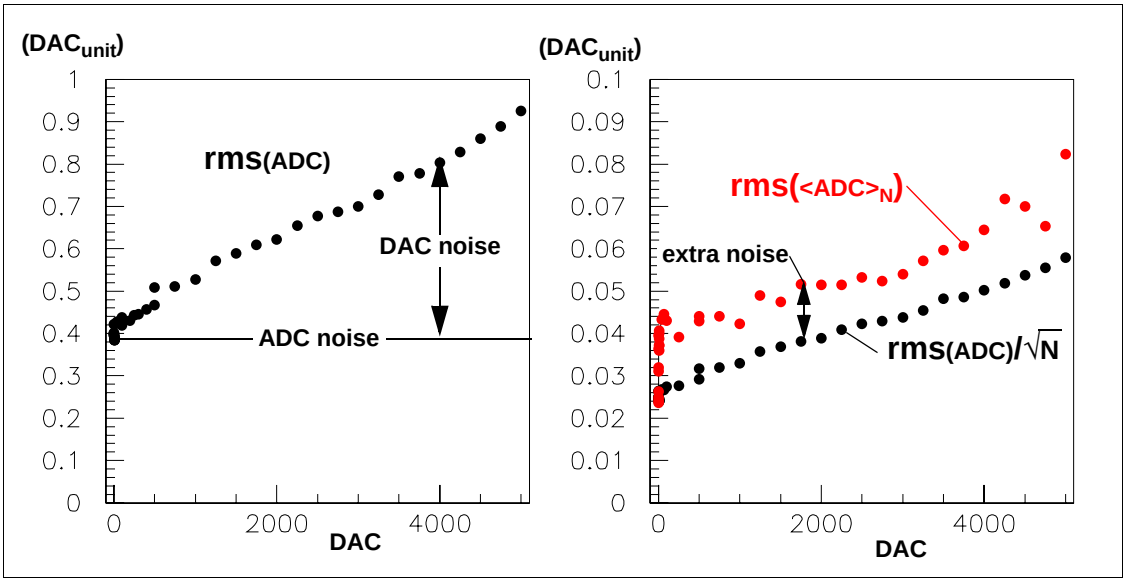

Figure 4: On the left plot we represent the noise affecting one ADC sample as a function of the DAC count. Our model consider that a constant part at 0.4 DAC_{unit} (=0.8 ADC_{unit}) is the ADC input noise and a part proportional to the DAC output is due to the DAC. Both noise being 'white' they are decreased by a factor 16 by averaging ADC samples during 8.5 ms (N=256 samples). This operation revels another 'extra noise' component (maybe 50hz) at a 0.015 DAC_{unit} level, which sets a limit to what can be gained by the averaging procedure.

LED current itself. The precision of this measurement being better than a tenth of a DAC unit, i.e. $2*10^{-5}$ at mid scale, we have not tried to improve it by more averaging but we use it at frequencies below 1 hz to monitor various DC drifts during long 'level runs' or 'pedestal runs'.
During long runs we observe a drift of the mean value of LED current. In Figure 5 we represents these drifts as a function of the LED temperature (on the left for the pedestal value obtained by switching off the led current and for 4 different runs, on the right for a 50 hours run at DAC=10 level). Our conclusion is that the LED temperature is not the primary cause of the drifts but more likely the temperature of the backend electronic box. We shall monitor this temperature in order to control this drift at the 1% adu level.

3.2.3 LED thermal model

A complete thermal model can be drawn from records such as shown in Figure 6. The main information is that the thermal contact between a LED and the radiator behind acting as a thermal sink is sufficiently good to have an immediate rise (few seconds) of

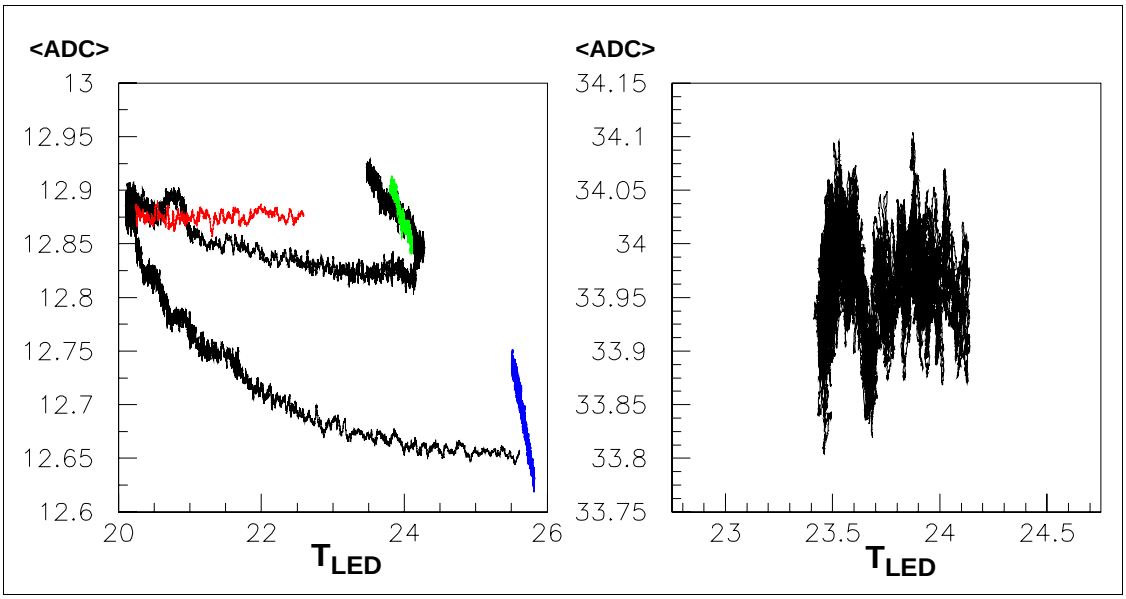

Figure 5: Monitoring LED current (V_L) during runs with varying LED temperature (T_{LED}). In the left figure LED switch is off and four different are superimposed (different colours); in the right figure DAC level is maintained at a small level (DAC=10)

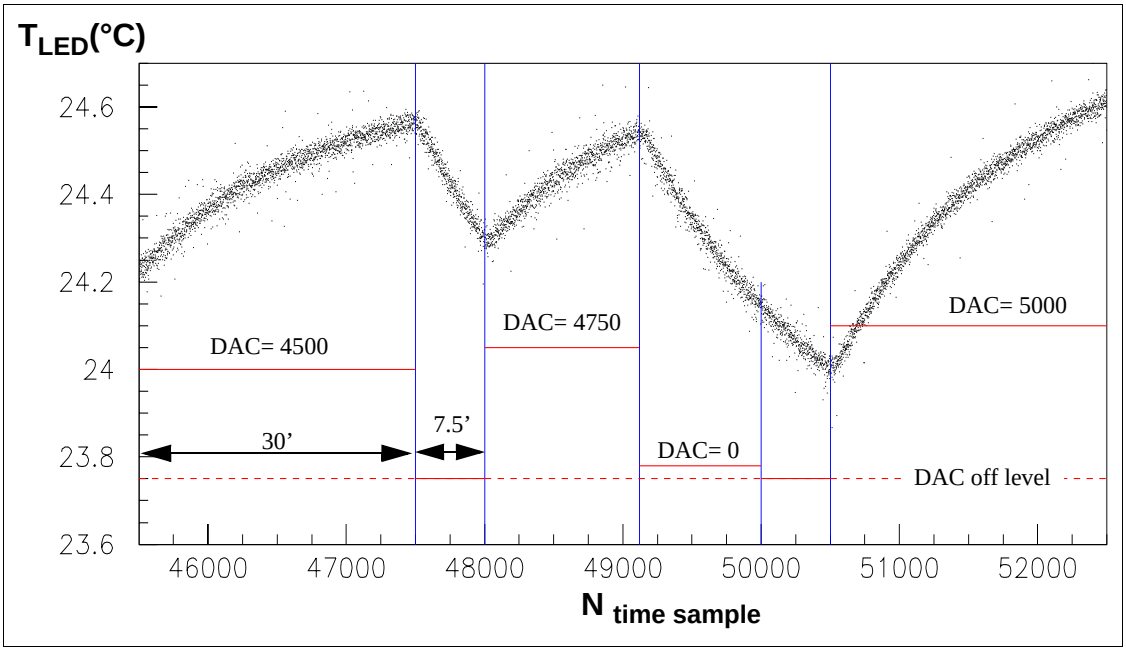

Figure 6: Evolution of the LED radiator temperature with time (sampling period 0.9 s). In red evolution of power disipated in LED GD8 (5000 DAC units is 160 mW). A vertical blue line mark each power change.

the radiator temperature T_{LED} for each change of power dissipated inside LED, so that we can consider that T_{LED} is the LED temperature. Moreover it takes 5' to have a rise of T_{LED} of 0.1 °C, which is the level for which a change of LED emission characteristic can be detected at the 10^{-4} level (cf. report LPNHE 2009-01).

4 Test of Photodiode readout electronics

When taking ‘final calibration data’ for our LED light source we discovered an unanticipated problem hereafter refered as the «photovoltaic question». We had purchased a NIST calibrated photodiode which arrived after the installation of SNDICE in Hawaii. A precalibration of SNDICE has been done before with a DKD calibrated diode. Our hope was to recalibrate the DKD diode with the more accurate NIST diode and to update the calibration of SNDICE, while studying how to use the high reliability of our bench to push to the limits the accuracy of our calibration method. The NIST method, contrary to ours[5], is ‘photovoltaic’, which means -unbiased diode, at room temperature, reading the ‘short circuit current’ I_{SC} using a feedback picoammeter-. For the immediate needs of SNDICE we have used a procedure compatible with the methods of calibration institutes and tried to control them empirically. On this basis we obtained a first recalibration of SNDICE based on a comparison of NIST and DKD efficiencies and many results in this report and (spectral,...). In parallel we started a dedicated investigation of photovoltaic versus photoelectric detector which is from our point of view essential before dealing with absolute calibration and photometric linearity.

4.0.1 the photovoltaic question from a physics point of view

The NIST practice of using an unbiased warm photodiode as a calibrated detector is opposite to the usual recommendations for a solid state photon or ionisation detector. The maker of the photodiode (Hamamatsu) recommends the use of the photoelectric mode because of the non-linearity and the lower sensitivity of the photovoltaic detectors and provides for the detection of a low light flux the Peltier cooled photodiodes that we are using. In the case of silicon photodiodes or CCDs it is well known that the good efficiency in the IR region is obtained due to a large bias depleting a thick intrinsic zone. After gaining some experience with unbiased photodiodes read by a feedback picoammeter we were surprised to see that results were better than expected although they suffer many problems. We solved them empirically depending notably on the picoammeter range used (i.e. the different analog constants used) and the detector capacitance. However a detailed experimental study is needed. We have initiated such a study using our CLAP electronics to understand the role of the feedback picoammeter which makes the system very different from a real photovoltaic model. Let us just recall the physics perspective: Charge collection in the Shockley photovoltaic model is a slow diffusion process driven by chemical gradient which raises voltage across the junction and dumps current in a passive external load, while a picoammeter is developping a fast voltage feedback drifting charges through the detector, using the capacitive feedback as seen in our analysis of CLAP (LPNHE 2007-01).

4.0.2 Empirical description of the LED-photodiode characteristic

We represent in Figure 7 the LED-photodiode characteristic for a high current, high efficiency LED (GD8). This curve is compounding the photon emission, the photon

[5] expressed in ref.EB-NIM and used for our CLAP detector

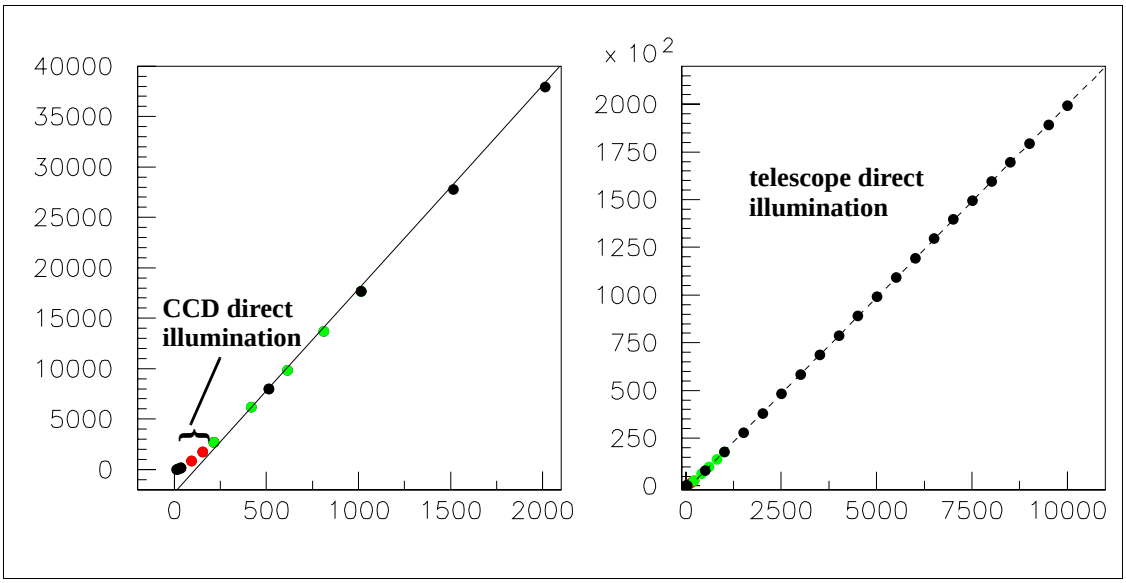

Figure 7: Photodiode current (pA) versus led-GD8 current (adu) characteristic. A linear fit in the range 2000<adu<10000 is superimposed (residuals are shown in Figure 11). The upper two-thirds of GD8 current range are not represented (I_{max}=500 mA ↔32000 adu) : the light flux is too high for the direct illumination of a telescope.

detection efficiencies and eventually the variability of the serial resistor R_L. The led current includes the shunt current which should be a constant if the diode threshold is sharp. The reasonable assumption that the emission probability is proportional to the current traversing the diode explains the linearity of the characteristic seen in Figure 7. The residuals of a linear fit seen in Figure 11, show that this hypothesis is very good except for the lower 10% of the range. We would like to model the non linear behaviour of this curve at low current, but we have to wait solving the photovoltaic question. But first we have to solve measurement inconsistencies (§4.0.3) and then understand current fluctuations (§4.0.4).

4.0.3 Inconsistencies of various photocurrent and noise measurements using our picoammeter

Figure 8 compares the picoammeter readings obtained with the 200 pA range with those of the 20 nA and 200 nA. It is surprising to see how big (30%) and reproductible is the difference. Even more surprising are the fluctuations of a signal in the 200 pA range : a 4 fA resolution for the dark current (better than specified and comparable with CLAP's 3 fA/root(hz) resolution) but degraded by a factor 20 for 40 pA and by a factor 200 for 170 pA. This degradation of noise goes with the apparition of a second peak below or above the main gaussian peak. Our standard CCD calibrating flux being Φ_{std}=160 pA/cm2, we conclude that we have no reliable measurement of calibrated photodiode signal in the crucial range needed for CCD calibration.

4.0.4 Low frequency (LF) fluctuations of the picoammeter measurement

1- Low intensity levels.

Our main monitoring frequency is 1.1 hz. The raw led and the photodiode signal are each

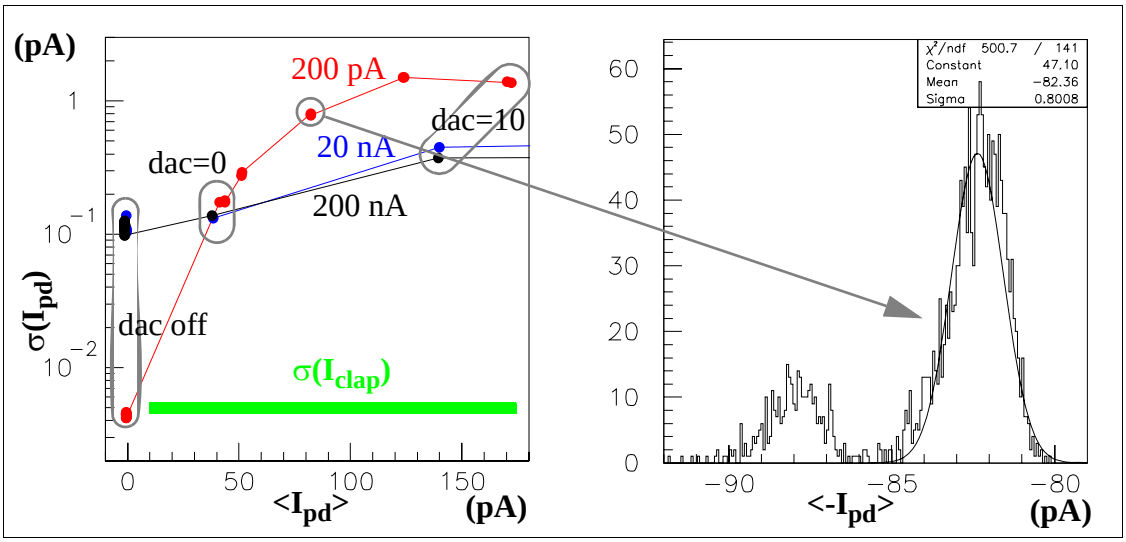

Figure 8: **left:** Comparison of photocurrent & noise read using different picoammeter ranges : red, blue and black for 200 pA, 20 nA and 200 nA. Points for identical dac levels are circled (off, 0, 10). **right:** Histogram shows the bimodal noise distribution appearing in the 200 pA range

sampled during 0.1 s within this .9 s period. This corresponds for the led to 500 ADC cycles and for the picoammeter to 5 PLC (power line cycle). Both could be made more precise by a factor 3 to 10 by suppressing undersampling. The distribution of 100 consecutive samples (1.5') is shown to be gaussian white (except for the 200 pA current range). Averaging 100 samples has boosted precision by an order of magnitude to permit the analyses shown in Figure 9. The left figure shows that the picoammeter pedestal is

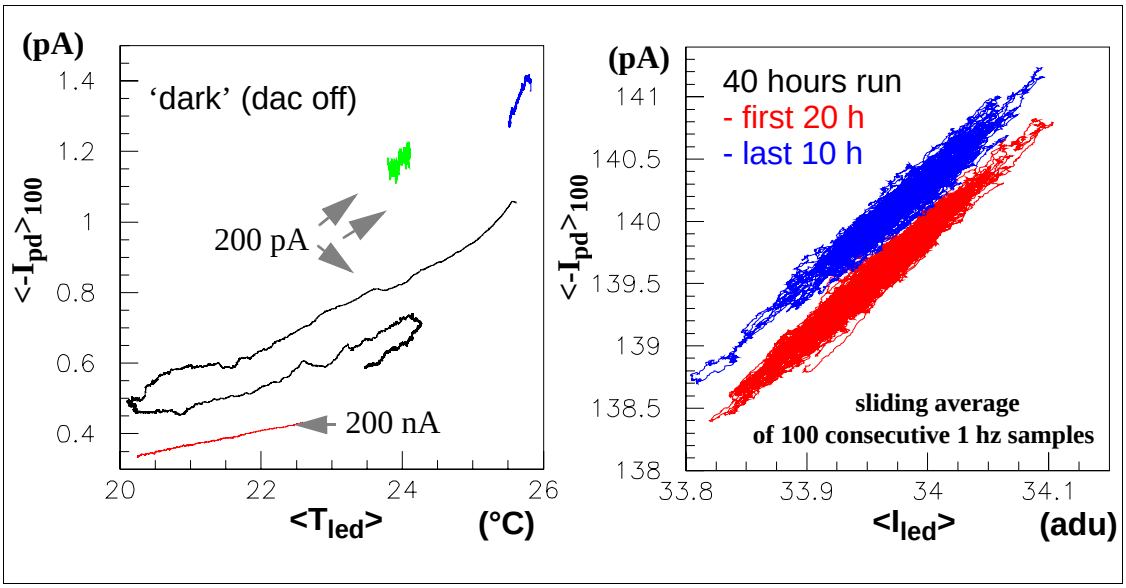

Figure 9: **left :** temperature dependence of picoammeter pedestal (pA and nA ranges) **right:** fluctuations of low level photocurrent correlated with led current fluctuations (DAC=10)

temperature dependent but with other perturbations to be identified. The right figure shows that the origin of most photocurrent LF noise at low level is light intensity fluctuation due to the electric fluctuation in the LED. An extra perturbation factor at very

low frequency is shown by the evolution of pedestal during a long run. We can suppress these effects using the I_{led} monitor to correct the picoammeter measurement. This is shown in Figure 10.

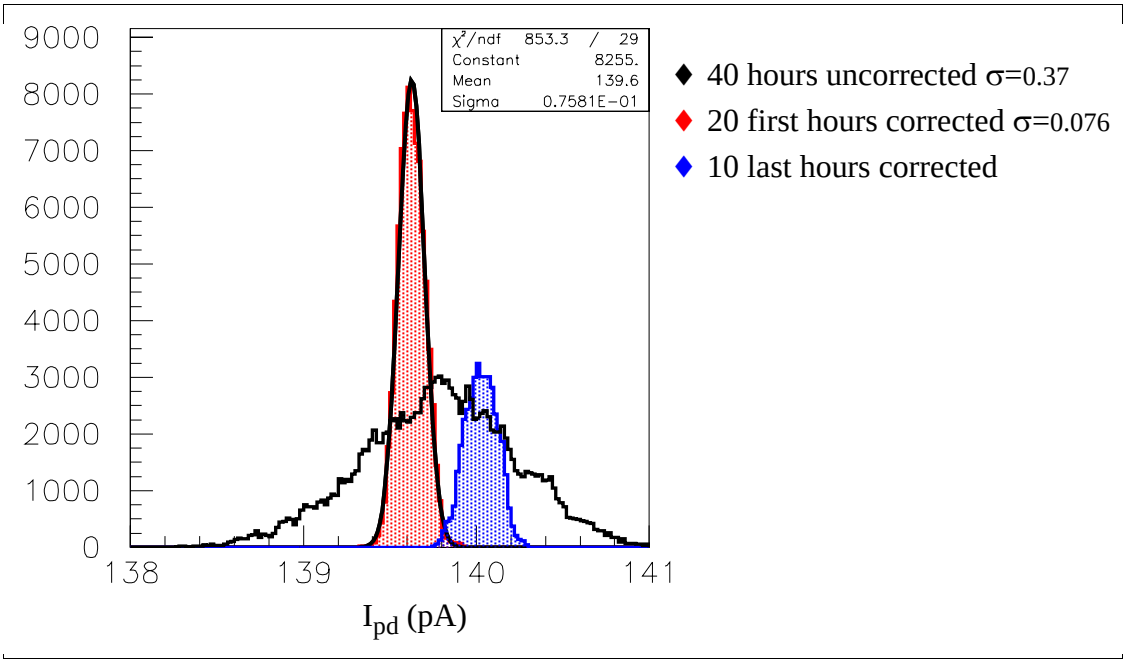

Figure 10: The effect of the correction procedure using current monitoring to improve the flux resolution of the photodiode measurement is displayed : the 0.25% resolution is enhanced to $5*10^{-4}$

-2- High intensity levels.

Figure 11 represent the essential features defining the quality of the LED light source

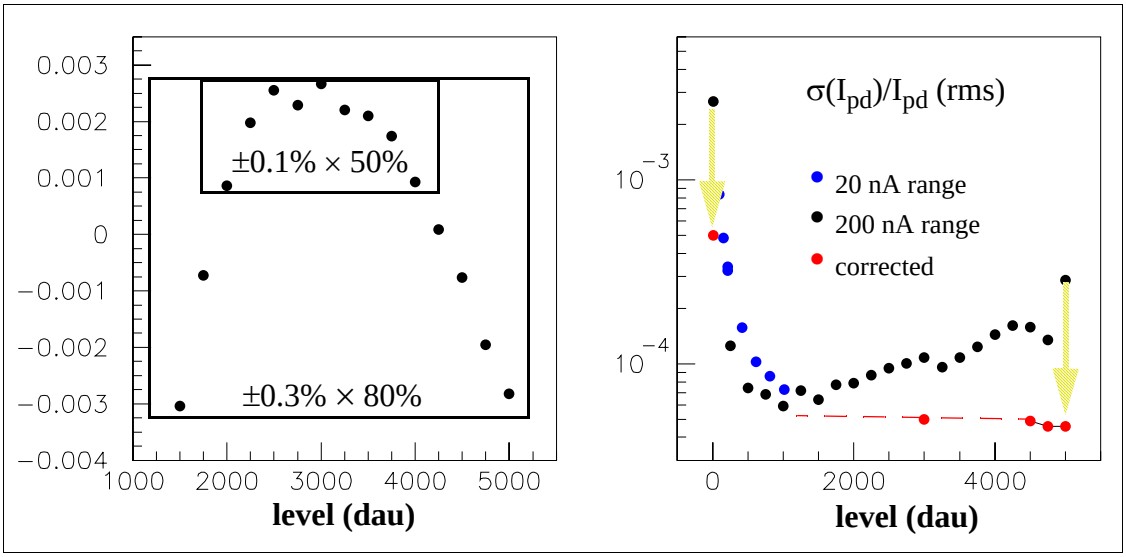

Figure 11: **left :** residuals of a linear fit of $I_{pd}(I_{led})$ give two boxes ±0.1% over 50% and ±0.3% over 80% of the DAC range (temperature correction on high level points have not been made)
right : photocurrent fluctuations are ≈10^{-4} on the central DAC range. Two corrections (↓) reduce these fluctuations on both extremities of the range (explained in Figure 10 and Figure 12)

along the range of DAC values.
Firstly in Figure 11-left the residuals to a linear fit which are shown to be contained within a ±0.1% box for half of the range and within ±0.3% above the lower 20% of the range. Deviation from linearity could come from LED emission, from photodiode detection (particularly in the photovoltaic mode), from the R_L resistor or from the picoammeter electrical calibration. The stability of the LED yield at the 10^{-4} level has been tested once for a week and more commonly for one or two days. It showed that LED temperature correction has to be taken into account at this precision (and that no other correction is needed). Therefore an empirical light yield model of the LED source, linear at the 10^{-2} level, can be tabulated at 10^{-4} level as a function of led current and temperature and progressively one will root out its detector dependence.
Secondly in Figure 11-right we see the fluctuations of the photodiode GD8 current at 1 hz frequency monitored continuously during 30' for DAC level varying from 10 to 5000. This is the most significant data qualifying the precision of our source for common photometry experiments (in addition of Figure 3 which show the gradation of the light flux scale in 16384 equal intervals). The relative precision, at 10^{-4} level between DAC=1000 to DAC=4000, degrades in the low intensity region (even after the improvement shown in Figure 10) and in the high intensity region. This last effect is easily understood as a variation of light yield (0.18%/°C) due to the rise of the LED radiator temperature due to the LED self-heating (cf. Figure 12). It is corrected down to

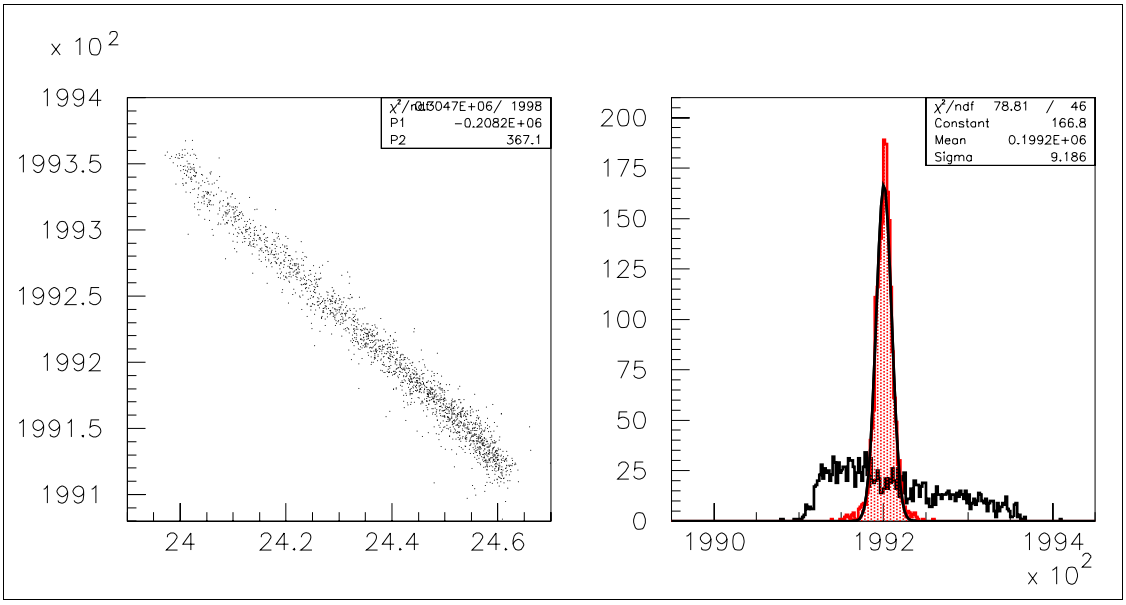

Figure 12: **left :** led yield vs led temperature (led radiator temperature rises when led is continuously on). The yield decreases by 0.18%/°C.
right : linear correction of temperature reduces the dispersion of photocurrent at dac=5000 to 5.10^{-5}

$0.5*10^{-4}$ using the LED temperature monitor and it gives a precise measurement of the light yield thermal coefficient. However it is not a significant effect in itself because in normal telescope illumination the average power dissipated in LED is not sufficiently important by two order of magnitude to act on the led yield.

Thirdly the extension of this study to higher DAC levels was carried over in another run and revealed two other problems:

- Extra picoammeter noise. Photodiode currents above the 200 nA limit require the 2 µA picoammeter range. Repeating the DAC=5000 measurement of Figure 12 with the 2 µA range, yielded the result shown in Figure 13.

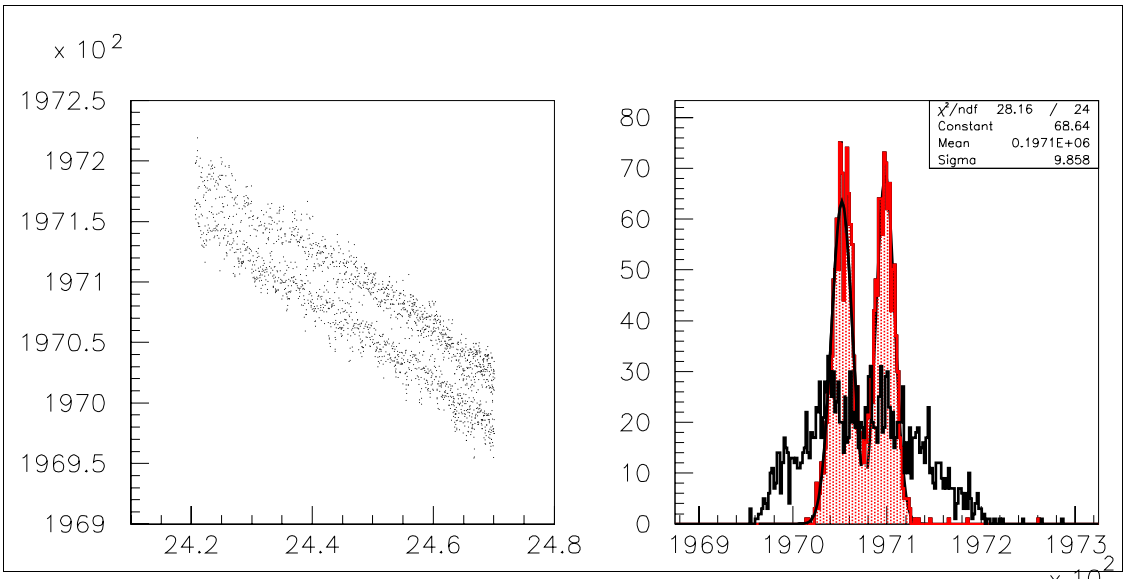

Figure 13: Same as Figure 12, but using 2 µA picoammeter range instead of 200 nA range. An extra noise is introduced by the picoammeter

- Power limit of led current source: In Figure 14, we see that our current controller is

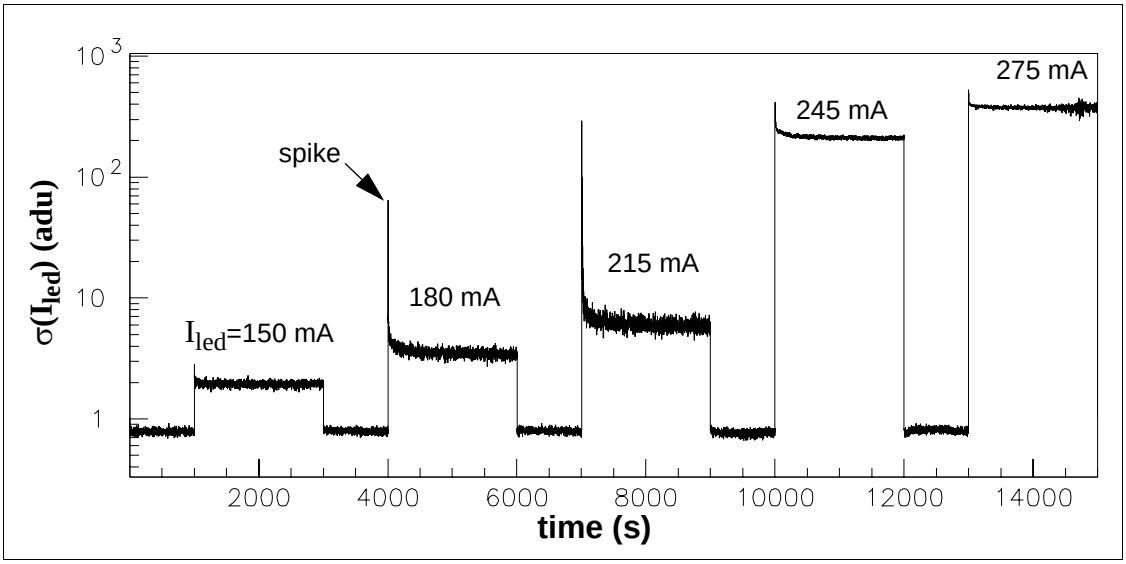

Figure 14: RMS fluctuation of LED current I_{led} when it is ramped from 150 to 275 mA. Power supply limits I_{led} to 300 mA (max allowed 500 mA). Instability of current controller in the khz frequency range appears above 150 mA (spikes at onset) and jumps above 215 mA without affecting the photodiode current.

limited practically to 300 mA and degrades above 200 mA.

5 A model of LED emission

A modern high intensity LED is an array of small semiconductor patches connected to an input point A by a metallic grid in order to minimize the access resistance to the light emitting region. The total access impedance includes shottky barrier, p and n doped semiconductor regions and eventually the double heterojunctions. A reasonable first order model representing LED properties, in particular the proportionality of LED current and photoelectric detector current, consist as in Figure 15, of introducing a

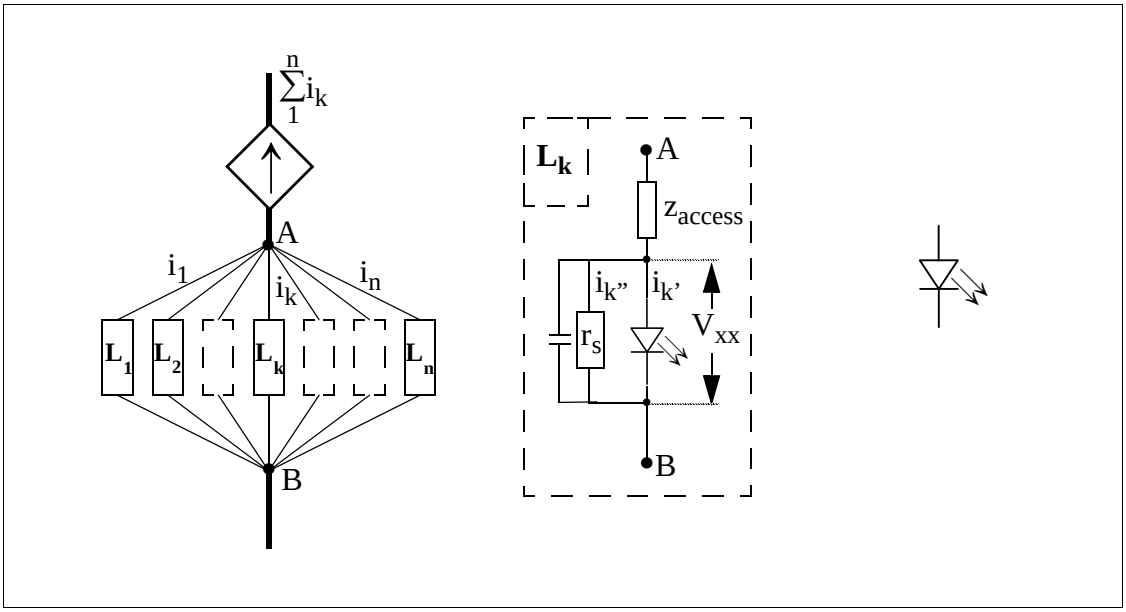

Figure 15: Representation of a LED as an array of single photon emitters (“nanoled”)

parallel array of independent emitting cells with similar current-voltage characteristics. The current i_k flowing through one cell is the sum of a diode current i_k' (null for $V<V_{xx}$) and a shunt current i_k''.

6

7 Conclusions

Concerning the SNDICE light source hardware, our conclusions are particularly optimistic. We do not see much improvement needed. The current source controller is obviously too weak to control a LED current above 200 mA and much better than expected at very low current. Considering the needs for the monitoring of the Megacam CCD camera (expressed in Table 1), we have to modify the ballast resistors in order to limit maximum currents to 200 mA (or less) instead of 500 mA. This extends by the same amount the **lower limit of flux stability**[6]. These limits can be independently

[6] a 10^{-3} limit and a 10^{-4} limit can be easily defined from Figure 11

improved by a factor two by using the 2.5 volt DAC reference (instead of 1.25) and by doubling the ballast resistors. All these modifications needing a recalibration of the SNDICE source, they will be done in due time. We have also proposed another modification concerning the low current cutoff of the led current source seen in Figure 3 at 10 adu (which is attributed to the offset of the current defining transistor) and a temperature monitoring of the electronics. These requests are not related to the SNDICE specifications, but to ours. Their goal is to yield a high precision light source for studying the photodetector efficiency and its linearity in a very large range of flux including very low values. Our present study was restricted to calibrated photodiodes at room temperature read by a commercial picoammeter. We have been confined to the nA picoammeter ranges, after observing that pA and µA ranges were not performing well. In the nA range the picoammeter photocurrent noise is two order of magnitude higher than our CLAP noise, with the effect that our results depend heavily on averaging while single photocurrent measurement is possible. In the CLAP electronics study we have been able to examine the role of every meaningful parameter: detector capacitance, preamp feedback capacitance and resistance, input transistor, intermediate analog filters, final digitization and digital filter, various noises sources. A general purpose instrument, for instance our picoammeter, does not have the same flexibility.

Appendix A:Quoted from H1 report November 2nd 1990

How to Deal with $\sigma_{noise} < 1$ (adu)

E.BARRELET *LPNHE*

Abstract:
We expose the elementary mathematics needed to understand and correct a problem affecting the electronic calibration of H1 LAr, which turns out to be a rather general and widely ignored problem. It happens because the ADC digitization stage (adu) is close to σ (its gaussian electronic noise RMS), as a consequence of the optimization of the range covered by the electronic chain. More generally this type of effects must be taken in consideration when defining the number of ADC bits needed to cover a given voltage amplitude range and when one envisage to extend the bottom of the amplitude range by averaging many samples, often after adding an artificial electronic noise to the signal measured. In order to implement easily the results of this study we use essentially the classical mean and sigma estimators based on sums of samples and squared samples, in our case computed directly by our DSP readout.

7.1 Digitization of an analog channel with gaussian white noise

Appendix B: LED Backend Electronics

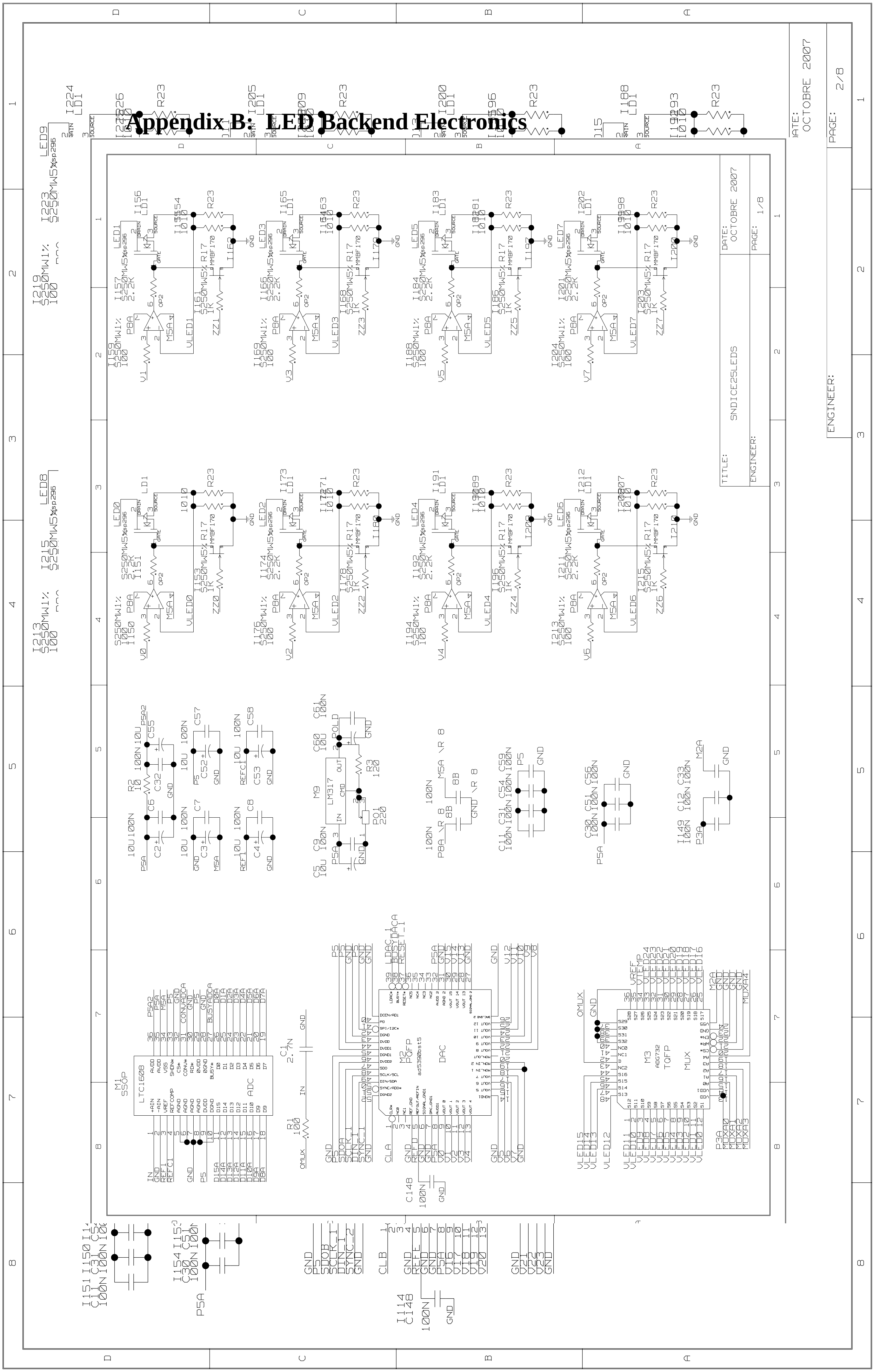

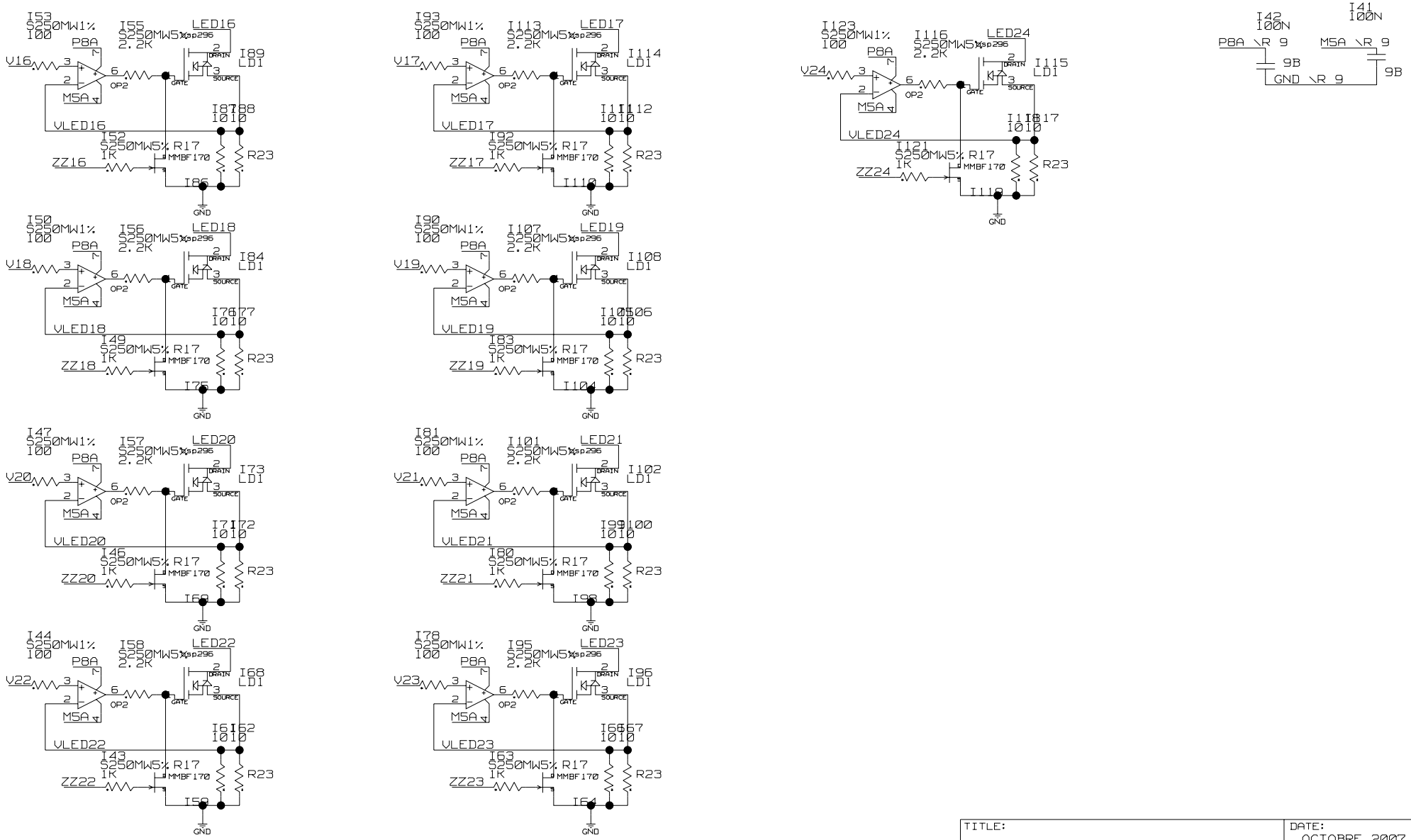
I53
S250MW1%
100
P8A
V16
M5A
OP2
I55
S250MW5%sp296
2.2K
LED16
I89
LD1
DRAIN
GATE
SOURCE
VLED16
I52
S250MW5%
1K
R17
MMBF170
ZZ16
R23
I86
GND
I50
S250MW1%
100
P8A
V18
M5A
OP2
I56
S250MW5%sp296
2.2K
LED18
I84
LD1
VLED18
I49
S250MW5%
1K
R17
MMBF170
ZZ18
R23
I75
GND
I47
S250MW1%
100
P8A
V20
M5A
OP2
I57
S250MW5%sp296
2.2K
LED20
I73
LD1
VLED20
I46
S250MW5%
1K
R17
MMBF170
ZZ20
R23
I68
GND
I44
S250MW1%
100
P8A
V22
M5A
OP2
I58
S250MW5%sp296
2.2K
LED22
I68
LD1
VLED22
I43
S250MW5%
1K
R17
MMBF170
ZZ22
R23
I59
GND
I93
S250MW1%
100
P8A
V17
M5A
OP2
I113
S250MW5%sp296
2.2K
LED17
I114
LD1
VLED17
I92
S250MW5%
1K
R17
MMBF170
ZZ17
R23
I110
GND
I90
S250MW1%
100
P8A
V19
M5A
OP2
I107
S250MW5%sp296
2.2K
LED19
I108
LD1
VLED19
I83
S250MW5%
1K
R17
MMBF170
ZZ19
R23
I104
GND
I81
S250MW1%
100
P8A
V21
M5A
OP2
I101
S250MW5%sp296
2.2K
LED21
I102
LD1
VLED21
I80
S250MW5%
1K
R17
MMBF170
ZZ21
R23
I98
GND
I78
S250MW1%
100
P8A
V23
M5A
OP2
I95
S250MW5%sp296
2.2K
LED23
I96
LD1
VLED23
I63
S250MW5%
1K
R17
MMBF170
ZZ23
R23
I64
GND
I123
S250MW1%
100
P8A
V24
M5A
OP2
I116
S250MW5%sp296
2.2K
LED24
I115
LD1
VLED24
I121
S250MW5%
1K
R17
MMBF170
ZZ24
R23
I118
GND
I41
100N
P8A \R 9
9B
I42
100N
M5A \R 9
9B
GND \R 9
TITLE:
DATE:
OCTOBRE 2007
ENGINEER:
PAGE:
3/8

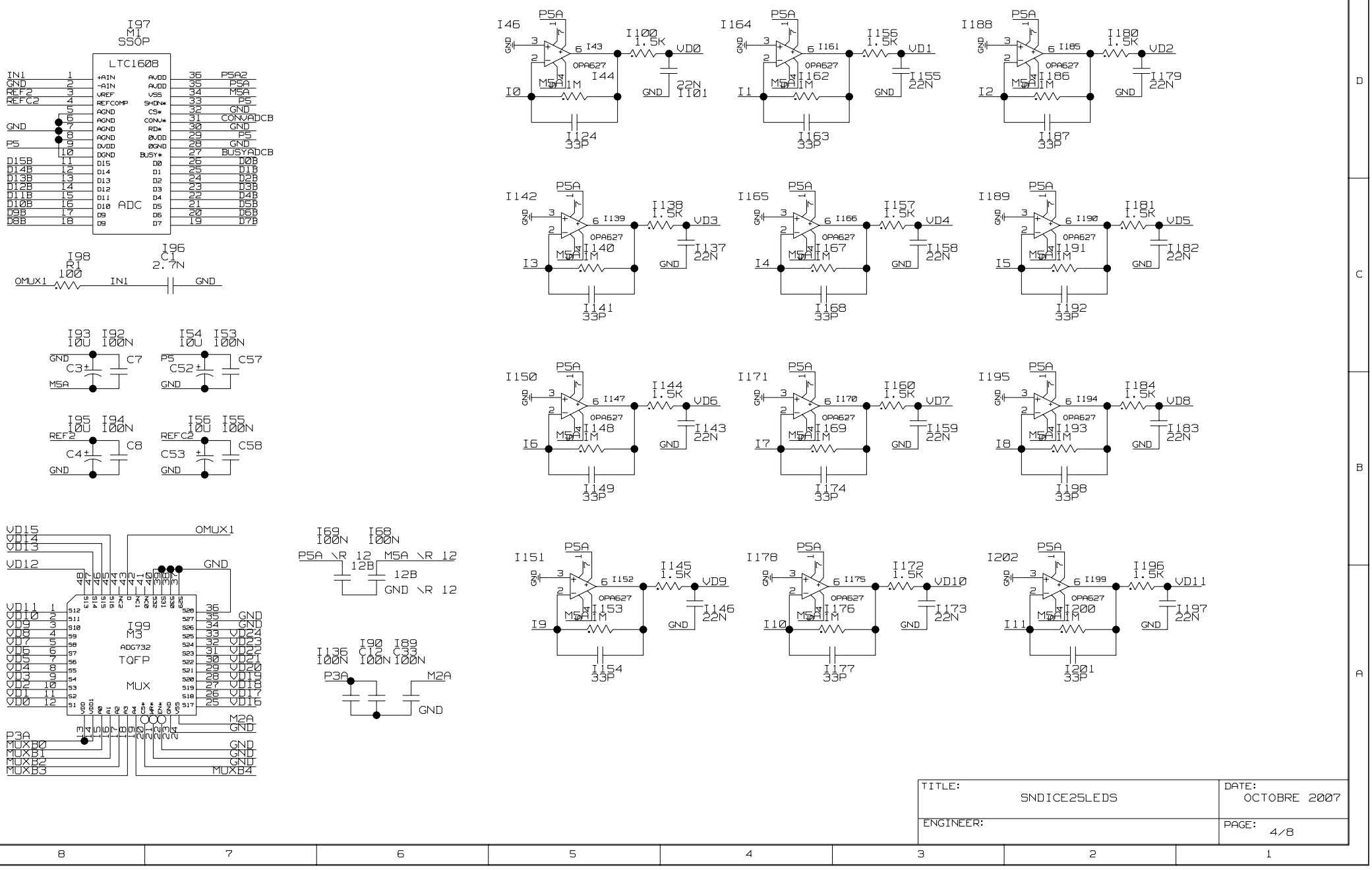

TITLE: SNDICE25LEDS	DATE: OCTOBRE 2007
ENGINEER:	PAGE: 4/8

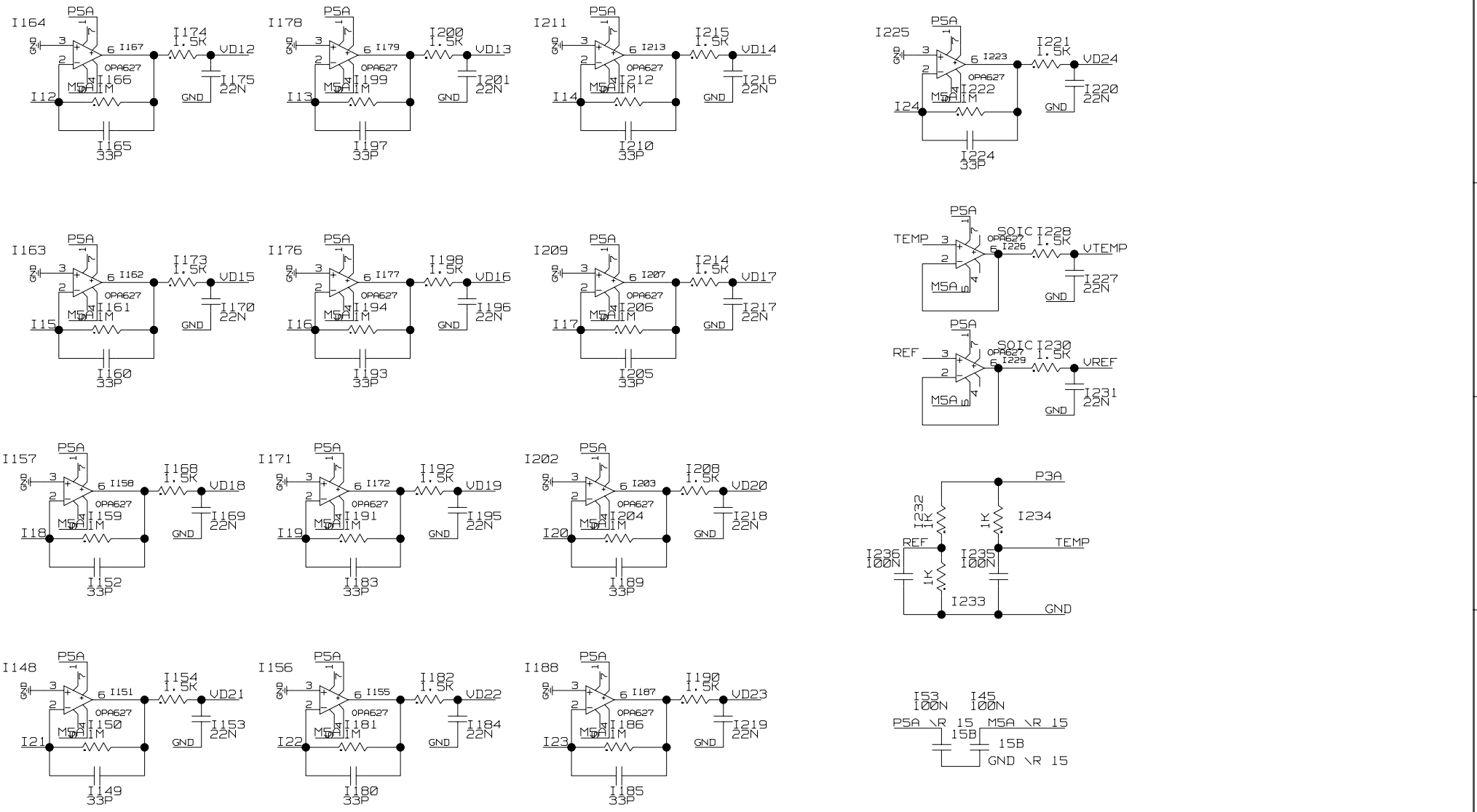
I164
P5A
I174
1.5K
VD12
I167
OPA627
I166
M5A
I12
I165
33P
I175
22N
GND
I178
P5A
I200
1.5K
VD13
I179
OPA627
I199
M5A
I13
I197
33P
I201
22N
GND
I211
P5A
I215
1.5K
VD14
I213
OPA627
I212
M5A
I14
I210
33P
I216
22N
GND
I225
P5A
I221
1.5K
VD24
I223
OPA627
I222
M5A
I24
I224
33P
I220
22N
GND
I163
P5A
I173
1.5K
VD15
I162
OPA627
I161
M5A
I15
I160
33P
I170
22N
GND
I176
P5A
I198
1.5K
VD16
I177
OPA627
I194
M5A
I16
I193
33P
I196
22N
GND
I209
P5A
I214
1.5K
VD17
I207
OPA627
I206
M5A
I17
I205
33P
I217
22N
GND
TEMP
P5A
SOIC
I228
1.5K
VTEMP
OPA627
I226
M5A
I227
22N
GND
REF
P5A
SOIC
I230
1.5K
VREF
OPA627
I229
M5A
I231
22N
GND
I157
P5A
I168
1.5K
VD18
I158
OPA627
I159
M5A
I18
I152
33P
I169
22N
GND
I171
P5A
I192
1.5K
VD19
I172
OPA627
I191
M5A
I19
I183
33P
I195
22N
GND
I202
P5A
I208
1.5K
VD20
I203
OPA627
I204
M5A
I20
I189
33P
I218
22N
GND
P3A
I232
1K
1K
I234
REF
TEMP
I236
100N
I235
100N
1K
I233
GND
I148
P5A
I154
1.5K
VD21
I151
OPA627
I150
M5A
I21
I149
33P
I153
22N
GND
I156
P5A
I182
1.5K
VD22
I155
OPA627
I181
M5A
I22
I180
33P
I184
22N
GND
I188
P5A
I190
1.5K
VD23
I187
OPA627
I186
M5A
I23
I185
33P
I219
22N
GND
I53
100N
I45
100N
P5A \R 15
15B
M5A \R 15
15B
GND \R 15
TITLE:
SNDICE25LEDS
DATE:
OCTOBRE 2007
ENGINEER:
PAGE:
5/8

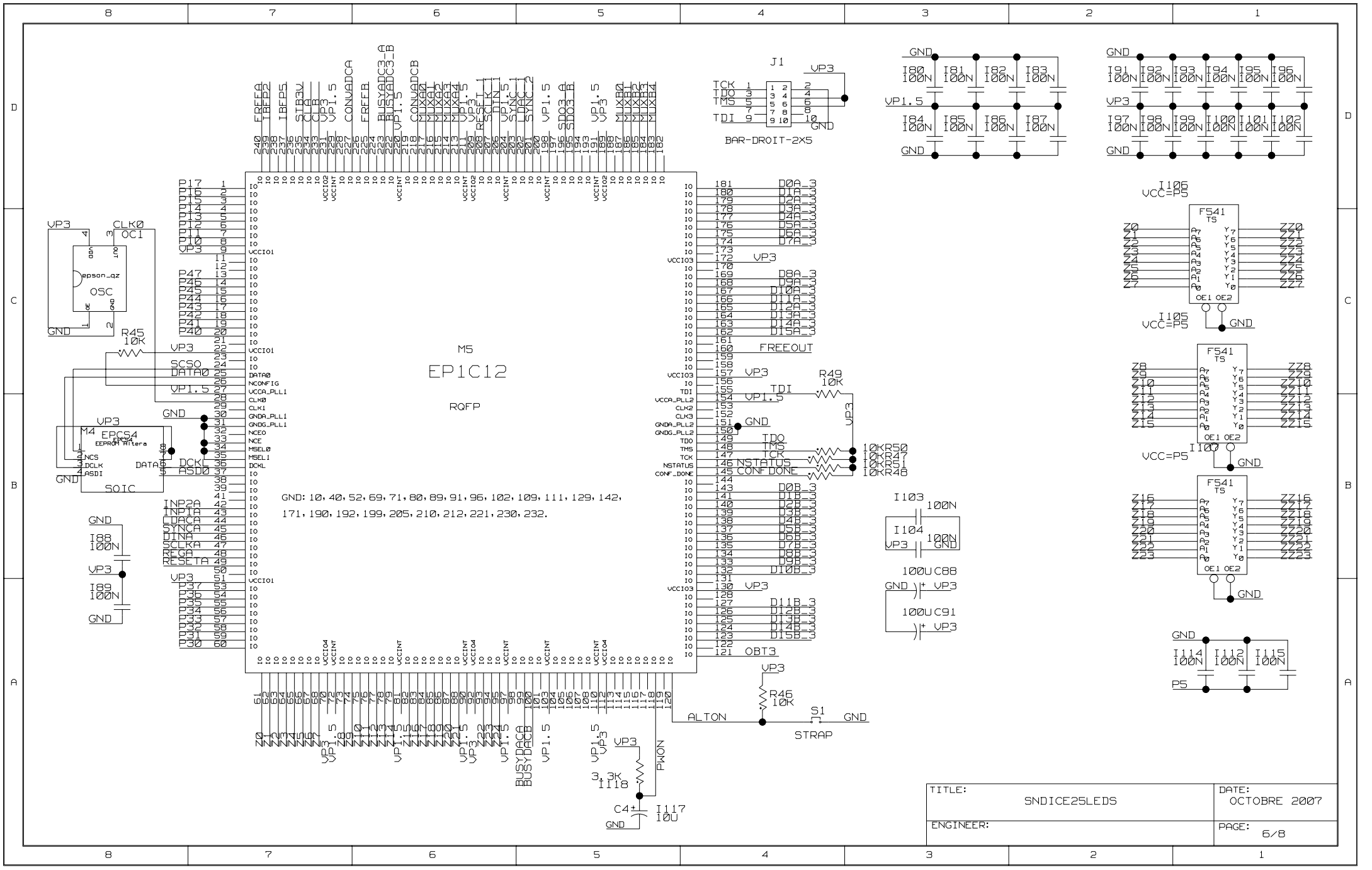
M5
EP1C12
RQFP
GND: 10, 40, 52, 69, 71, 80, 89, 91, 96, 102, 109, 111, 129, 142,
171, 190, 192, 199, 205, 210, 212, 221, 230, 232.
J1
BAR-DR01T-2X5
M4
EPCS4
SOIC
OSC
epson_qz
STRAP
F541
TS
TITLE:
SNDICE25LEDS
DATE:
OCTOBRE 2007
ENGINEER:
PAGE:
6/8

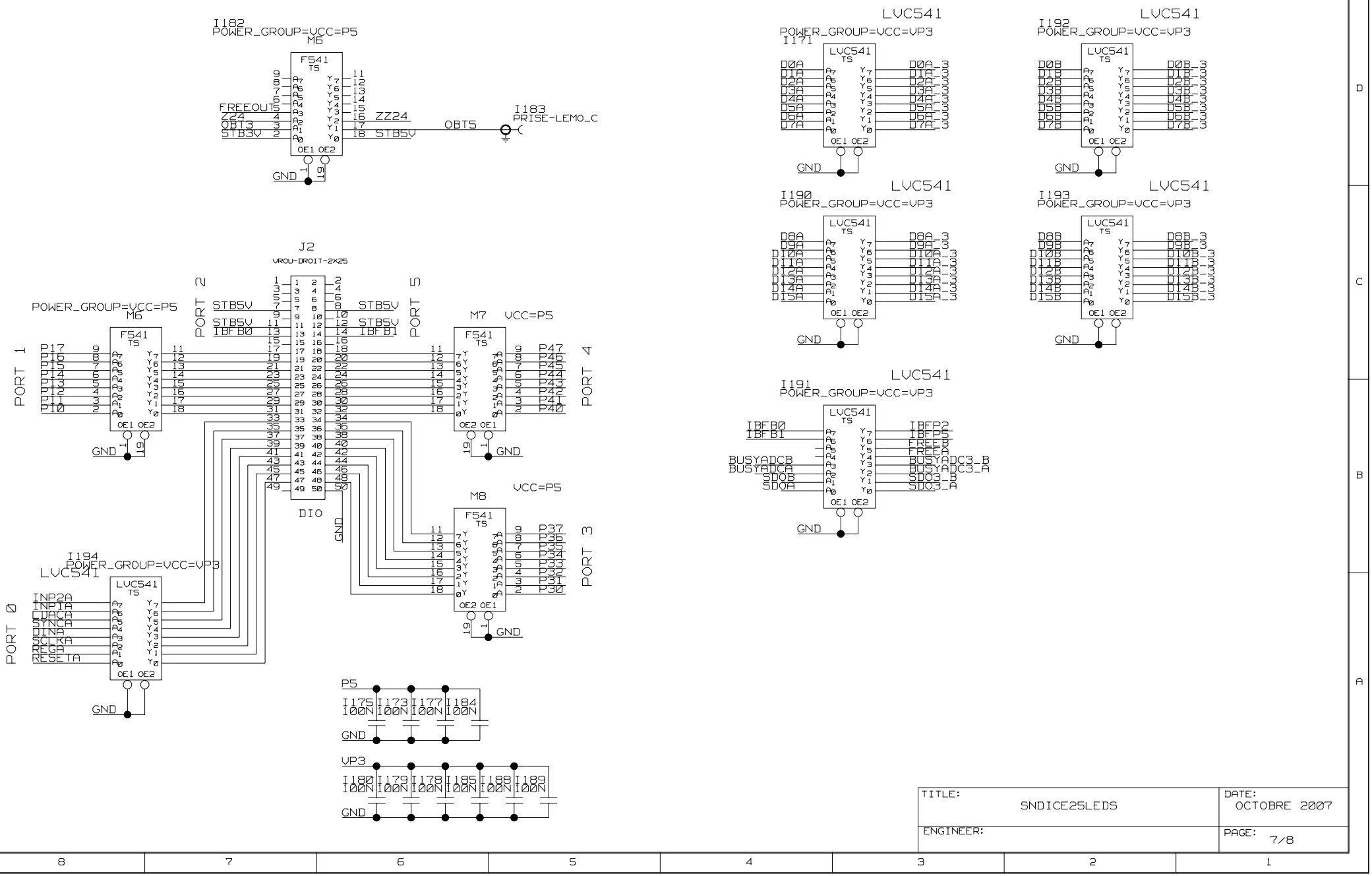
I182
POWER_GROUP=VCC=P5
M6
F541
TS
FREEOUT5
ZZ24
OBT3
STB3V
ZZ24
STB5V
OBT5
I183
PRISE-LEMO_C
GND
J2
VROU-DROIT-2X25
PORT 2
PORT 5
STB5V
IBFB0
IBFB1
POWER_GROUP=VCC=P5
M6
M7
VCC=P5
PORT 1
PORT 4
P17
P16
P15
P14
P13
P12
P11
P10
P47
P46
P45
P44
P43
P42
P41
P40
DIO
M8
VCC=P5
PORT 3
P37
P36
P35
P34
P33
P32
P31
P30
I194
POWER_GROUP=VCC=VP3
LVC541
LVC541
PORT 0
INP2A
INP1A
SYNCA
SYNCA
DINA
SCLKA
RFGA
RESETA
P5
I175
I173
I177
I184
I00N
VP3
I180
I179
I178
I185
I188
I189
LVC541
POWER_GROUP=VCC=VP3
I171
I192
I190
I193
I191
D0A
D1A
D2A
D3A
D4A
D5A
D6A
D7A
D0B
D1B
D2B
D3B
D4B
D5B
D6B
D7B
D8A
D9A
D10A
D11A
D12A
D13A
D14A
D15A
D8B
D9B
D10B
D11B
D12B
D13B
D14B
D15B
IBFB0
IBFB1
BUSYADCB
BUSYADCA
SDOB
SDOA
IBFP2
IBFP5
FREEB
FREEA
BUSYADC3_B
BUSYADC3_A
SDO3_B
SDO3_A
TITLE:
SNDICE25LEDS
DATE:
OCTOBRE 2007
ENGINEER:
PAGE:
7/8

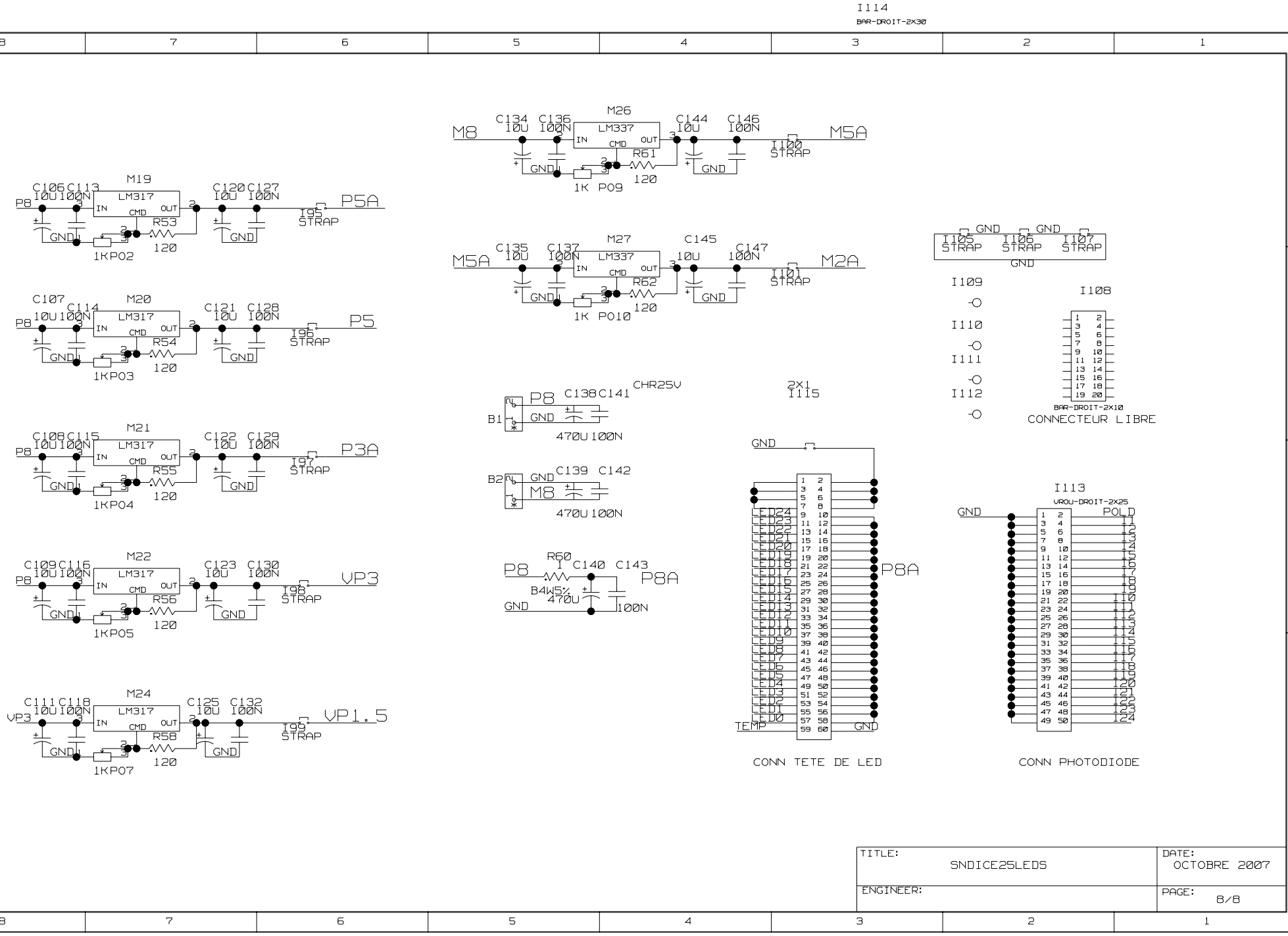
I114
BAR-DROIT-2X30
M19
C106 C113
10U 100N
LM317
IN CMD OUT
P8
GND
R53
120
1KP02
C120 C127
10U 100N
I95
STRAP
P5A
M20
C107 C114
C121 C128
I96
P5
R54
1KP03
M21
C108 C115
C122 C129
I97
P3A
R55
1KP04
M22
C109 C116
C123 C130
I98
VP3
R56
1KP05
M24
C111 C118
C125 C132
I99
VP1.5
R58
1KP07
M26
C134 C136
C144 C146
M8
M5A
R61
1K P09
M27
C135 C137
C145 C147
M2A
R62
1K P010
I100
I101
I105
I106
I107
I109
I110
I111
I112
I108
BAR-DROIT-2X10
CONNECTEUR LIBRE
B1
C138 C141
CHR25V
470U 100N
B2
C139 C142
M8
R60
C140 C143
B4W5%
470U
100N
P8A
2X1
I115
TEMP
CONN TETE DE LED
I113
VROU-DROIT-2X25
POLD
CONN PHOTODIODE
TITLE:
SNDICE25LEDS
DATE:
OCTOBRE 2007
ENGINEER:
PAGE:
8/8